Gravitational lensing by hairy black holes in Einstein-scalar-Gauss-Bonnet theories

Yuan-Xing Gao[1] and Yi Xie[1,2,*]

[1]*School of Astronomy and Space Science, Nanjing University, Nanjing 210023, China*
[2]*Key Laboratory of Modern Astronomy and Astrophysics, Nanjing University, Ministry of Education, Nanjing 210023, China*

(Received 8 December 2020; accepted 22 January 2021; published 12 February 2021)

We investigate the weak and strong deflection gravitational lensing by the hairy black holes in the Einstein-scalar-Gauss-Bonnet (EsGB) gravity with five types of coupling functions (quadratic, cubic, quartic, inverse-polynomial, and logarithmic), which can evade the no-hair theorem. The lensing observables are found and the possibility of detecting the effects of the scalar hair is analyzed. We find that all of the shadows cast by these black holes are consistent with the measurement by the Event Horizon Telescope, while other lensing observables are beyond the present capacity. Therefore, it is currently impossible to distinguish these black holes from the Schwarzschild one and from each other merely by their lensing signatures, leaving testing the EsGB gravity by gravitational lensing until new technology is available.

DOI: 10.1103/PhysRevD.103.043008

I. INTRODUCTION

Inspired by the low energy effective string theory [1,2], an Einstein-scalar-Gauss-Bonnet (EsGB) theory is of great interest, because its nonminimal coupling between the Gauss-Bonnet invariant and a dynamical scalar field can avoid Ostrogradski instability or ghosts [3,4] and it has richer phenomena than Einstein's general relativity (GR) does. As a subclass of the EsGB gravity, an Einstein-dilaton-Gauss-Bonnet (EdGB) theory has its scalar field with shift symmetry representing the dilaton [5]. Such a theory can possess hairy black hole solutions [6,7]. It was recently realized that, beyond the shift symmetry, the EsGB theory with appropriately chosen coupling functions connecting the Gauss-Bonnet invariant and the scalar field might also allow for the existence of black hole solutions with the scalar hair [8–18].

In contrast with black holes in GR, these hairy EsGB black holes might have interesting and different features, since the scalar hair could change in a very large range. Therefore, it is necessary to confront theoretical predictions of these black holes with empirical observation for better understanding of the EsGB gravity. For observation via gravitational waves, the quasinormal modes of the hairy black holes have been widely investigated [19–21]. It was also found [22] that the hairy black holes in the EsGB theory satisfy current constraints on the speed of gravitational waves constrained by GRB 170817A and GW170817 [23,24]. For observations via electromagnetic waves, the shadow cast by a hairy black hole in the EdGB theory was studied by a numerical method and it was found that it is always smaller than that of a Kerr black hole with the same mass and angular momentum under similar observation conditions [25]. The shadows of the hairy black holes in the EsGB theory with other coupling functions were examined [26] by using the analytic expressions for their metrics with the method of the continued-fraction approximation [27]. It was claimed [26] that the analytic expressions are matched with the numerical ones very well within ∼1% and the scalar hair can make the shadows bigger than that of the Schwarzschild black hole. However, gravitational lensing signatures of these hairy black holes are barely known and relevant studies are still absent, requiring a detailed investigation.

Gravitational lensing has been an invaluable tool for providing insights on spacetimes [28]. In the weak deflection scenario, the bending angle is much less than 1 and its lensed images can be routinely observed in practice. The weak deflection gravitational lensing has been intensively studied and employed in astronomy [29–32] and in gravitational physics [33–39]. In the strong deflection scenario, the bending angle is much bigger than 1 so that a photon can round a black hole by more than one circle. The strong deflection gravitational lensing results in an escape cone of light or "shadow" [40], relativistic images [41] (see Refs. [42,43] for reviews) and photon rings [44–46]. The shadow of the supermassive black hole M87* has been directly imaged by the Event Horizon Telescope (EHT) and its diameter was measured as about 42 microarcsecond (μas) [47–52], leading to tests beyond the first post-Newtonian order [53] (see further discussion in Refs. [54,55]) and of the black hole geometry in the vicinity of the circular photon orbit [55]. Nevertheless, the relativistic images and photon rings

*yixie@nju.edu.cn

are currently inaccessible due to their tiny separation and exceeding faintness [56,57] and very narrow width [44–46]. If the relativistic images and photon rings would be accessible in the future with the help of new technology, such as a space interferometry, they could be beneficial for understanding black holes [56,58–61], searching and distinguishing different kinds of them [62–66], and providing a precise gravitational test in the strong field [67].

Motivated by these considerations and taking the advantage of combining the weak and strong deflection gravitational lensing to provide a whole picture [68–74], we will investigate these two complementary kinds of gravitational lensing by the hairy black holes in the EsGB theory in the present work for understanding their full lensing signatures.

The paper is organized as follows. In Sec. II, the spacetime for the hairy EsGB black holes is briefed and the generic setup for the gravitational lensing is reviewed. We obtain the observables in the weak deflection gravitational lensing by the hairy black holes in Sec. III, including positions, magnifications, and time delays of the lensed images, and discuss their observability by taking the supermassive black hole in the Galactic Center Sgr A* as lens. The observables in the strong deflection gravitational lensing, such as the apparent radius of the shadow as well as the angular separation, brightness difference, and time delays between the relativistic images are found out in Sec. IV. By taking Sgr A* and M87* as lenses, their observability is estimated and analyzed. We conclude and discuss our results in Sec. V.

II. BLACK HOLES IN ESGB GRAVITY AND GRAVITATIONAL LENSING

A. Black holes in EsGB gravity

A general theory of EsGB gravity reads ($G = c = 1$) [10–12]

$$S = \frac{1}{16\pi}\int \mathrm{d}^4x\sqrt{-g}\left[R - \frac{1}{2}\nabla_\mu\phi\nabla^\mu\phi + \tilde{\alpha}f(\phi)R^2_{\mathrm{GB}}\right], \quad (1)$$

where $\tilde{\alpha}$ is the coupling constant, $f(\phi)$ is the coupling function, and R^2_{GB} is the Gauss-Bonnet invariant

$$R^2_{\mathrm{GB}} = R^2 - 4R_{\mu\nu}R^{\mu\nu} + R_{\mu\nu\rho\sigma}R^{\mu\nu\rho\sigma}. \quad (2)$$

It admits black hole solutions which might evade the no-hair theorem [10–12]. While these solutions have generally been found by numerical methods [10–12], we consider their representation under the continued-fraction approximation [27] because such an analytic method of approximation has sufficient accuracy compared to the numerical methods and it provides an easier way to apply. Under the continued-fraction approximation, the static and spherically symmetric black hole solutions valid from the event horizon to the infinity were obtained as [26]

$$\mathrm{d}s^2 = -A(r)\mathrm{d}t^2 + B(r)\mathrm{d}r^2 + r^2(\mathrm{d}\theta^2 + \sin^2\theta\mathrm{d}\varphi^2), \quad (3)$$

where

$$A(r) = 1 - \frac{2M}{r} + \frac{8M^3(a_1 + a_2\epsilon)}{a_2(1+\epsilon)^3r^3} - \frac{8M^3a_1}{a_2[(1+\epsilon)(1+a_2)r - 2Ma_2)](1+\epsilon)^2r^2}, \quad (4)$$

$$B(r) = \frac{1}{A(r)}\left\{1 + \frac{4M^2b_1}{[(1+\epsilon)(1+b_2)r - 2Mb_2](1+\epsilon)r}\right\}^2, \quad (5)$$

and the r-dependent scalar field was found as [26]

$$\phi(r) = \phi_\infty + \log\left\{1 + \frac{2Mf_0}{(1+\epsilon)r} + \frac{4M^2f_1}{[(1+\epsilon)(1+f_2)r - 2Mf_2](1+\epsilon)r}\right\}. \quad (6)$$

Here, M is the asymptotic mass of the black hole and ϕ_∞ is the asymptotic value of the scalar field. The continued-fraction coefficients $\{\epsilon, a_1, a_2, b_1, b_2, \phi_\infty, f_0, f_1, f_2\}$ rely on the specific choice of the form of $f(\phi)$, whereas all of them are the functions of $p \in [0,1]$ [26]. Following the convention of Ref. [26] that chooses to fix $4\tilde{\alpha}r_{\mathrm{h}}^{-2} = 1$, where r_{h} is the radius of the event horizon, p is defined as

$$p = 6\dot{f}(\phi_{\mathrm{h}})^2, \quad (7)$$

where ϕ_{h} is the value of the scalar field evaluated at the event horizon of the black hole and a dot denotes the derivative with respect to ϕ. Based on five types of coupling functions of the EsGB gravity that are quadratic, cubic, quartic, inverse-polynomial, and logarithmic ones $f(\phi) = \{\phi^2, \phi^3, \phi^4, \phi^{-1}, \log(\phi)\}$, their continued-fraction coefficients have been worked out in Ref. [26] and they are adopted and shown in the Appendix for completeness and convenience. Although p can more easily parametrize the continued-fraction coefficients, it has less physical meaning than ϕ_{h}. It was found [26] that the specific form of $f(\phi)$ also determines the range of ϕ_{h}, which is quite different from each other among the five coupling functions. When ϕ_{h} is non-negative,

(i) $\phi_{\mathrm{h}} \in [0, 24^{-1/2}]$ for $f(\phi) = \phi^2$;
(ii) $\phi_{\mathrm{h}} \in [0, 54^{-1/4}]$ for $f(\phi) = \phi^3$;
(iii) $\phi_{\mathrm{h}} \in [0, 96^{-1/6}]$ for $f(\phi) = \phi^4$;
(iv) $\phi_{\mathrm{h}} \in [6^{1/4}, +\infty)$ for $f(\phi) = \phi^{-1}$;
(v) $\phi_{\mathrm{h}} \in [6^{1/2}, +\infty)$ for $f(\phi) = \log(\phi)$.

In order to describe ϕ_{h} in a unified manner for all of the coupling functions, we define a normalized indicator ξ as

$$\xi = \frac{\phi_{\mathrm{h}} - \phi_{h,\min}}{\phi_{h,\max} - \phi_{h,\min}}, \quad (8)$$

where $\phi_{h,\min}$ and $\phi_{h,\max}$ are the minimum and maximum values for the ϕ_h. Since ϕ_h for $f(\phi) = \{\phi^{-1}, \log(\phi)\}$ can reach infinity, we set a sufficiently large cutoff on its absolute value as $\phi_{h,\max} = 30$.

In the weak field limit, the metric functions $A(r)$, $B(r)$, and the scalar field $\phi(r)$ can be expanded as [10,12,14,75]

$$A(r) = 1 - \frac{2M}{r} + \frac{Q^2}{12}\left(\frac{M}{r}\right)^3 + \mathcal{O}\left(\frac{M}{r}\right)^4, \tag{9}$$

$$B(r) = 1 + \frac{2M}{r} + \frac{16 - Q^2}{4}\left(\frac{M}{r}\right)^2 + \frac{32 - 5Q^2}{4}\left(\frac{M}{r}\right)^3 + \mathcal{O}\left(\frac{M}{r}\right)^4, \tag{10}$$

$$\phi(r) = \phi_\infty + Q\frac{M}{r} + Q\left(\frac{M}{r}\right)^2 + \frac{32Q - Q^3}{24}\left(\frac{M}{r}\right)^3 + \mathcal{O}\left(\frac{M}{r}\right)^4, \tag{11}$$

where Q is a dimensionless parameter defined by the ratio of the mass of the black hole to its scalar charge and the continued-fraction approximation of Q is [26]

$$Q = \frac{2f_0}{1+\epsilon}. \tag{12}$$

It is distinct that Q only depends on ϵ and f_0 and $A(r)$ and $B(r)$ reduce to those of the Schwarzschild black hole as Q vanishes. Figure 1 shows Q with respect to p and ξ in its top and bottom panels. When Q is parametrized by p (see top panel in Fig. 1), the curves of Q for $f(\phi) = \{\phi^3, \phi^4\}$ (in green and orange) almost coincide with each other so that it is hard to tell their maximum absolute difference about 7×10^{-4}. However, when Q is parametrized by ξ (see bottom panel in Fig. 1), these two curves are separated by a narrow but clear gap. It well demonstrates the mathematical convenience of p and the physical clearness of ξ.

In the following investigation on gravitational lensing, the metric (3) with the continued-fraction approximated (4) and (5) will be used for the strong deflection gravitational lensing to take the strong field into account, while the one with the weak-field expansion (9) and (10) will be adopted for the weak deflection gravitational lensing since it is sufficient for the weak field.

B. Gravitational lensing

The exact bending angle of a light ray caused by the black hole in EsGB theory (3) is [76]

$$\hat{\alpha} = 2\int_{r_0}^{\infty} \frac{r_0\sqrt{A(r)B(r)}}{r\sqrt{r^2A(r_0) - r_0^2A(r)}}\mathrm{d}r - \pi, \tag{13}$$

where r_0 is the closest approach of the light ray and it relates to the impact parameter b by

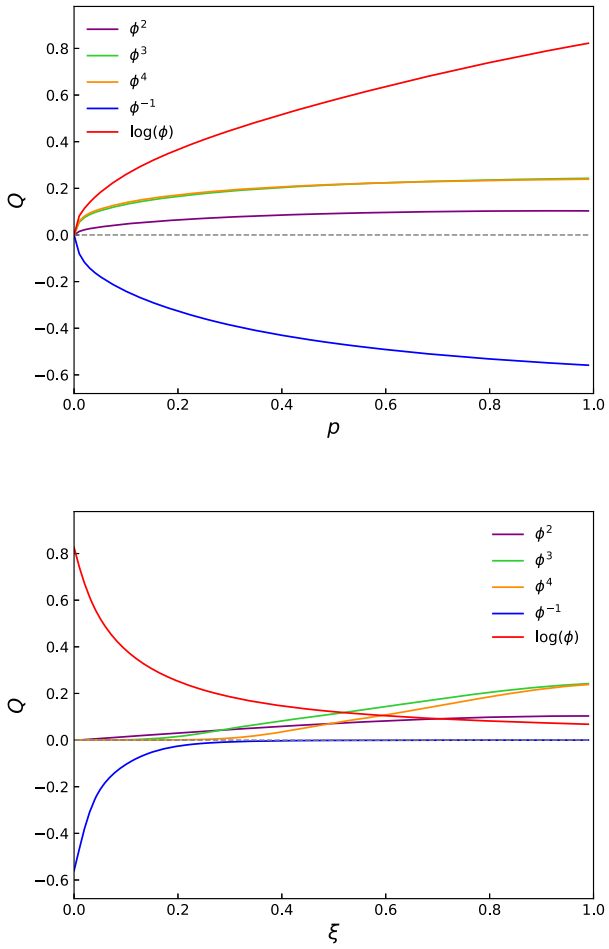

FIG. 1. Q against p (top) and ξ (bottom) for $f(\phi) = \{\phi^2, \phi^3, \phi^4, \phi^{-1}, \log(\phi)\}$.

$$r_0 = b\sqrt{A(r_0)}. \tag{14}$$

When r_0 is much larger than the gravitational radius $\sim 2M$ of the black hole, $\hat{\alpha}$ will be much smaller than 1 and the bending angle (13) can be handled by the small-angle approximation, resulting in weak deflection gravitational lensing. When r_0 is comparable with $\sim 2M$, $\hat{\alpha}$ will be much bigger than 1, giving the strong deflection gravitational lensing.

Finding lensing observables needs the lens equation, which describes the relation among the source, the lens, and the observer. We assume that the source and the observer are in the asymptotically flat regions of the lens so that the lens equation is taken as [58]

$$\tan\mathcal{B} = \tan\vartheta - D[\tan\vartheta + \tan(\hat{\alpha} - \vartheta)], \tag{15}$$

where $\mathcal{B}$ is the angular position of the source, $\vartheta = \arcsin(bd_{\mathrm{L}}^{-1})$ is the angular position of the image with d_{L} being the distance from the lens to the observer, and $D = d_{\mathrm{LS}}/d_{\mathrm{S}}$ with d_{LS} and d_{S} being the distances, respectively, from the lens to the source and from the source to the

observer. The magnification of a lensed image at the angular position ϑ is defined as [77]

$$\mu(\vartheta) = \left[\frac{\sin\mathcal{B}(\vartheta)}{\sin\vartheta}\frac{\mathcal{B}(\vartheta)}{d\vartheta}\right]^{-1}. \tag{16}$$

Furthermore, if the brightness of the source is changing, it would be able to measure the time delay between the lensed images. The time delay of a lensed image is given by the difference between the light travel time with and without the lens [33]

$$\tau = T(R_{\rm src}) + T(R_{\rm obs}) - \frac{d_{\rm S}}{\cos\mathcal{B}}, \tag{17}$$

where $R_{\rm src} = \sqrt{d_{\rm LS}^2 + d_{\rm S}^2\tan^2\mathcal{B}}$, $R_{\rm obs} = d_{\rm L}$, and the function $T(R)$ is

$$T(R) = \int_{r_0}^{R} \frac{r\sqrt{A(r_0)B(r)}}{\sqrt{A(r)[r^2A(r_0) - r_0^2A(r)]}}{\rm d}r. \tag{18}$$

These formulas lay the foundations of the following investigation on the weak and strong deflection gravitational lensing by the hairy black holes in EsGB theory.

III. WEAK DEFLECTION GRAVITATIONAL LENSING

A. Bending angle

In the weak field, the impact parameter b slightly deviates from r_0 because $A(r_0)$ is close to 1 when $r_0 \gg 2M$. Therefore, after expanding the right-hand side of Eq. (14) in powers of Mb^{-1} by using Eq. (9), we can find

$$r_0 = b\left[1 - \left(\frac{M}{b}\right) - \frac{3}{2}\left(\frac{M}{b}\right)^2 - \left(4 - \frac{Q^2}{24}\right)\left(\frac{M}{b}\right)^3 + \mathcal{O}\left(\frac{M}{b}\right)^5\right]. \tag{19}$$

Then, following the procedure proposed in Ref. [33], we can obtain the bending angle for the weak deflection gravitational lensing by the hairy EsGB black hole as

$$\hat{\alpha}(b) = 4\left(\frac{M}{b}\right) + \left(\frac{15\pi}{4} - \frac{\pi Q^2}{16}\right)\left(\frac{M}{b}\right)^2 + \left(\frac{128}{3} - \frac{4Q^2}{3}\right)\left(\frac{M}{b}\right)^3 + \mathcal{O}\left(\frac{M}{b}\right)^4. \tag{20}$$

Since the existence of Q diminishes the coefficients of $M^n b^{-n}$ $(n \geq 2)$, such a bending angle will always be smaller than the one of the Schwarzschild black hole.

B. Image positions, magnifications, and time delay

For the sake of convenience, we make the following rescaling [33]:

$$\beta = \frac{\mathcal{B}}{\vartheta_{\rm E}}, \quad \theta = \frac{\vartheta}{\vartheta_{\rm E}}, \quad \varepsilon = \frac{\vartheta_{\bullet}}{\vartheta_{\rm E}}, \quad \hat{\tau} = \frac{\tau}{\tau_{\rm E}}, \tag{21}$$

where $\vartheta_{\rm E}$ is the angular Einstein ring radius as

$$\vartheta_{\rm E} = \sqrt{\frac{4MD}{d_{\rm L}}}, \tag{22}$$

$\vartheta_{\bullet} = \tan^{-1}(M/d_{\rm L})$ is the angular gravitational radius of the black hole, τ is the time delay, and $\tau_{\rm E}$ is the characteristic scale for the time delay

$$\tau_{\rm E} = 4M. \tag{23}$$

It is assumed that both the source and the observer are sufficiently far from the lens in the weak deflection gravitational lensing so that ε can be treated as a small parameter.

Therefore, the image position can be expanded into a series

$$\theta = \theta_0 + \varepsilon\theta_1 + \varepsilon^2\theta_2 + \mathcal{O}(\varepsilon^3), \tag{24}$$

where $\theta_{0,1,2}$ are the zero-, first-, and second-order approximation of the image position. Substituting Eq. (24) into the lens equation (15) and making use of the bending angle (20), we can find the image position order by order in terms of ε as

$$\theta_0 = \frac{1}{2}(\eta + \beta), \tag{25}$$

$$\theta_1 = \frac{\pi(60 - Q^2)}{64(1 + \theta_0^2)}, \tag{26}$$

$$\theta_2 = \frac{1}{\theta_0(1+\theta_0^2)^3}\left\{16 - \frac{225}{256}\pi^2 + \left(32 - \frac{225}{128}\pi^2\right)\theta_0^2 - 16D\theta_0^2(1+\theta_0^2)^2 + \frac{8D^2}{3}(1+\theta_0^2)^2(-2 + 6\theta_0^2 + \theta_0^4) + \frac{Q^2}{1536}[45\pi^2(1+2\theta_0^2) - 512(1+\theta_0^2)^2] - \frac{\pi^2Q^4}{4096}(1+2\theta_0^2)\right\}, \tag{27}$$

where

$$\eta = \sqrt{4 + \beta^2}. \tag{28}$$

The scalar field does not affect the leading term of the image position θ_0 but it changes its first- and second-order terms which reduce to those of the Schwarzschild black hole at $Q = 0$. Following the convention of Ref. [33] that the angular positions of the lensed images are positive, we can obtain the positive- and negative-parity images by setting $\beta = \pm|\beta|$ that

$$\theta_0^{\pm} = \frac{\eta \pm |\beta|}{2}, \tag{29}$$

$$\theta_1^{\pm} = \frac{\pi(60 - Q^2)}{32\eta(\eta \pm |\beta|)}, \tag{30}$$

$$\begin{aligned}\theta_2^{\pm} = {} & \frac{1}{\eta^3(\eta \pm |\beta|)^4}\left[1024 - \frac{675\pi^2}{16} - \frac{225\pi^2\beta^2}{16} + 768\beta^2 + 128\beta^4 - 128D(8 + 18\beta^2 + 8\beta^4 + \beta^6) + \frac{64}{3}D^2(40 + 134\beta^2\right. \\ & \left. + 79\beta^4 + 16\beta^6 + \beta^8) + Q^2\left(\frac{45\pi^2}{32} - \frac{64}{3} + \frac{15\pi^2\beta^2}{32} - 16\beta^2 - \frac{8}{3}\beta^4\right) - \frac{\pi^2Q^4}{256}(3 + \beta^2)\right] \\ & \pm \frac{|\beta|}{\eta^2(\eta \pm |\beta|)^4}\left[512 - \frac{675\pi^2}{48} + 128\beta^2 - 128D(8 + 6\beta^2 + \beta^4) + \frac{64}{3}D^2(52 + 53\beta^2 + 14\beta^4 + \beta^6)\right. \\ & \left. + Q^2\left(\frac{15\pi^2}{32} - \frac{32}{3} - \frac{8}{3}\beta^2\right) - \frac{\pi^2Q^4}{256}\right].\end{aligned} \tag{31}$$

Using a similar procedure, the magnification μ of a lensed image can be also found as a series according to ε

$$\mu = \mu_0 + \varepsilon\mu_1 + \varepsilon^2\mu_2 + \mathcal{O}(\varepsilon^3), \tag{32}$$

where

$$\mu_0 = \frac{\theta_0^4}{\theta_0^4 - 1}, \tag{33}$$

$$\mu_1 = -\frac{\pi\theta_0^3(60 - Q^2)}{64(1 + \theta_0^2)^3}, \tag{34}$$

$$\begin{aligned}\mu_2 = {} & \frac{\theta_0^2}{(\theta_0^2 - 1)(\theta_0^2 + 1)^5}\left[-32\theta_0^2 - 64\theta_0^4 + \frac{675\pi^2\theta_0^4}{128}\right. \\ & - 32\theta_0^6 - 32D\theta_0^2(1 + \theta_0^2)^2 \\ & + \frac{8D^2}{3}(1 + \theta_0^2)^2(1 + 16\theta_0^2 + \theta_0^4) \\ & + \frac{2Q^2}{3}\left(\theta_0^2 + 2\theta_0^4 - \frac{135\pi^2}{512}\theta_0^4 + \theta_0^6\right) \\ & \left. + \frac{3\pi^2Q^4}{2048}\theta_0^4\right],\end{aligned} \tag{35}$$

while the magnifications for the positive- and negative-parity images are, respectively, given by

$$\mu_0^{\pm} = \frac{1}{2} \pm \frac{2 + \beta^2}{2|\beta|\eta}, \tag{36}$$

$$\mu_1^{\pm} = -\frac{\pi(60 - Q^2)}{64\eta^3}, \tag{37}$$

$$\begin{aligned}\mu_2^{\pm} = {} & \pm\frac{1}{|\beta|\eta^5}\left[\frac{675\pi^2}{128} - 128 - 32\beta^2 - 32D(4 + \beta^2)\right. \\ & + \frac{8D^2}{3}(72 + 22\beta^2 + \beta^4) \\ & \left. + \frac{Q^2}{3}\left(8 + 2\beta^2 - \frac{135\pi^2}{256}\right) + \frac{3\pi^2Q^4}{2048}\right].\end{aligned} \tag{38}$$

Like the image position, the influence of the scalar field begins to manifest from the first-order term of the magnification.

If the two lensed images are unable to be practically resolved, the total magnification of them and their magnification-weighted centroid position will be the observables. The total magnification is defined as

$$\begin{aligned}\mu_{\text{tot}} & \equiv |\mu^+| + |\mu^-| \\ & = (2\mu_0^+ - 1) + 2\varepsilon^2\mu_2^+ + \mathcal{O}(\varepsilon^3),\end{aligned} \tag{39}$$

and the centroid is given by

$$\begin{aligned}\Theta_{\text{cent}} = {} & \frac{\theta^+|\mu^+| - \theta^-|\mu^-|}{|\mu^+| + |\mu^-|} \\ = {} & |\beta|\frac{\beta^2 + 3}{\beta^2 + 2} + \varepsilon^2\frac{|\beta|}{\eta^2(\beta^2 + 2)^2}\left[128 - \frac{675\pi^2}{128} + 32\beta^2\right. \\ & - 16D\beta^2(4 + \beta^2) + \frac{8D^2}{3}(-8 + 34\beta^2 + 13\beta^4 + \beta^6) \\ & \left. Q^2\left(-\frac{8}{3} + \frac{45\pi^2}{256} - \frac{2\beta^2}{3}\right) - \frac{3\pi^2Q^4}{2048}\right].\end{aligned} \tag{40}$$

Since the first-order terms of μ_{tot} and Θ_{cent} cancel out, Q merely appears in their second-order terms which would be hard to detect.

With the same scheme we used above, the time span function $T(R)$, see Eq. (18), can also be worked out

$$T(R) = \sqrt{R^2 - r_0^2} + r_0\left(\frac{\sqrt{1-\rho^2}}{1+\rho} + 2\log\frac{1+\sqrt{1-\rho^2}}{\rho}\right)\left(\frac{M}{r_0}\right) + r_0\left[\frac{15\pi}{4} - \frac{\pi Q^2}{16} - \frac{(4+5\rho)\sqrt{1-\rho^2}}{2(1+\rho)^2} - \left(\frac{15}{2} - \frac{Q^2}{8}\right)\sin^{-1}\rho\right]\left(\frac{M}{r_0}\right)^2 + \mathcal{O}\left(\frac{M}{r_0}\right)^3, \tag{41}$$

where

$$\rho = \frac{r_0}{R}. \tag{42}$$

Then we can obtain the time delay for the positive- and negative-parity images as

$$\hat{\tau}_\pm = \frac{\beta^2}{4} \pm \frac{|\beta|\eta}{4} - \frac{1}{2}\log\left(\frac{d_L\theta_0^{\pm 2}\vartheta_E^2}{4d_{LS}}\right) + \frac{\varepsilon\pi}{16\theta_0^\pm}\left(15 - \frac{Q^2}{4}\right) + \mathcal{O}(\varepsilon^2), \tag{43}$$

and have the differential time delay between these two images as

$$\Delta\hat{\tau} = \hat{\tau}_- - \hat{\tau}_+ = \frac{1}{2}|\beta|\eta + \log\left(\frac{\eta + |\beta|}{\eta - |\beta|}\right) + \frac{\varepsilon|\beta|\pi}{16}\left(15 - \frac{Q^2}{4}\right) + \mathcal{O}(\varepsilon^2). \tag{44}$$

If this delay is able to be measured up to its first-order level, it might put a potential upper bound on Q.

C. Practical observables

For practical measurements, the dimensionless and scaled quantities $\{\beta, \theta, \mu, \hat{\tau}\}$ must be converted to the physical ones $\{\mathcal{B}, \vartheta, F, \tau\}$ in which F is the observed flux of the image and $F = |\mu|F_{\rm src}$ with $F_{\rm src}$ being the unlensed flux of the source. Therefore, some measurable observables up to $\mathcal{O}(\varepsilon^2)$ can be constructed as [34]

$$P_{\rm tot} \equiv \vartheta^+ + \vartheta^- = \mathcal{E} + \varepsilon\frac{\vartheta_E\pi}{16}\left(15 - \frac{Q^2}{4}\right) + \mathcal{O}(\varepsilon^2), \tag{45}$$

$$\Delta P \equiv \vartheta^+ - \vartheta^- = |\mathcal{B}| - \varepsilon\frac{\vartheta_E|\mathcal{B}|\pi}{16\mathcal{E}}\left(15 - \frac{Q^2}{4}\right) + \mathcal{O}(\varepsilon^2), \tag{46}$$

$$F_{\rm tot} \equiv F^+ + F^- = \frac{2\vartheta_E^2 + \mathcal{B}^2}{|\mathcal{B}|\mathcal{E}}F_{\rm src} + \mathcal{O}(\varepsilon^2), \tag{47}$$

$$\Delta F \equiv F^+ - F^- = F_{\rm src}\left[1 - \varepsilon\frac{\pi\vartheta_E^3}{8\mathcal{E}^3}\left(15 - \frac{Q^2}{4}\right)\right] + \mathcal{O}(\varepsilon^2), \tag{48}$$

$$S_{\rm cent} \equiv \frac{\vartheta^+F^+ - \vartheta^-F^-}{F_{\rm tot}} = \frac{3\vartheta_E^2 + \mathcal{B}^2}{2\vartheta_E^2 + \mathcal{B}^2}|\mathcal{B}| + \mathcal{O}(\varepsilon^2), \tag{49}$$

$$\Delta\tau \equiv \tau_- - \tau_+ = \frac{d_L d_S}{d_{LS}}\left[\frac{|\mathcal{B}|\mathcal{E}}{2} + \vartheta_E^2\log\left(\frac{\mathcal{E} + |\mathcal{B}|}{\mathcal{E} - |\mathcal{B}|}\right) + \varepsilon\frac{\vartheta_E|\mathcal{B}|\pi}{16}\left(15 - \frac{Q^2}{4}\right) + \mathcal{O}(\varepsilon^2)\right], \tag{50}$$

where

$$\mathcal{E} = \sqrt{\mathcal{B}^2 + 4\vartheta_E^2}. \tag{51}$$

Their deviations from those of the Schwarzschild black hole can be indicated by

$$\delta P_{\rm tot} = P_{\rm tot} - P_{\rm tot,Sch} = -\varepsilon\frac{\pi\vartheta_E}{64}Q^2 + \mathcal{O}(\varepsilon^2), \tag{52}$$

$$\delta\Delta P = \Delta P - \Delta P_{\rm Sch} = \varepsilon\frac{\pi\vartheta_E|\mathcal{B}|Q^2}{64\mathcal{E}} + \mathcal{O}(\varepsilon^2), \tag{53}$$

$$\delta r_{\rm tot} = 2.5\log_{10}\left(\frac{F_{\rm tot}}{F_{\rm tot,Sch}}\right) = \mathcal{O}(\varepsilon^2), \tag{54}$$

$$\delta\Delta r = 2.5\log_{10}\left(\frac{\Delta F}{\Delta F_{\rm Sch}}\right) = \varepsilon\frac{5\pi\vartheta_E^3Q^2}{64\log(10)\mathcal{E}^3} + \mathcal{O}(\varepsilon^2), \tag{55}$$

$$\delta S_{\rm cent} = S_{\rm cent} - S_{\rm cent,Sch} = \mathcal{O}(\varepsilon^2), \tag{56}$$

$$\delta\Delta\tau = \Delta\tau - \Delta\tau_{\rm Sch} = -\varepsilon\frac{d_L d_S}{d_{LS}}\frac{\pi\vartheta_E|\mathcal{B}|Q^2}{64} + \mathcal{O}(\varepsilon^2). \tag{57}$$

The quantities with subscripts "Sch" mean their values for the Schwarzschild black hole which can be easily recovered by setting $Q = 0$. The existence of Q due to the scalar hair affects $P_{\rm tot}$, ΔP, ΔF, and $\Delta\tau$ at the level of $\mathcal{O}(\varepsilon)$ which might be able to measure, while its effects on $F_{\rm tot}$ and $S_{\rm cent}$ are both at the order of ε^2 which is expected to be far beyond the territory of current technology.

D. Example of Sgr A*

We estimate these observables in the weak deflection gravitational lensing by taking the supermassive black hole in the Galactic Center, Sgr A*, as the lens with $M = 4.28 \times 10^6\ M_\odot$ and $d_L = 8.32$ kpc [78], because stars orbiting Sgr A* have been regularly monitoring. We also assume a bright source with $d_{LS} = 6 \times 10^{-4}$ pc, which is roughly consistent with the periastron distance of the star S2 [78]. It leads to the angular Einstein radius as $\vartheta_E = 549\ \mu$as and the small parameter as $\varepsilon = 9.23 \times 10^{-3}$. For a reference, we can find the observables given by the Schwarzschild black hole as $P_{tot,Sch} = 1.147$ milliarcsecond (mas), $\Delta P_{sch} = 0.271$ mas, $\Delta F_{Sch}/F_{src} = 0.994$, and $\Delta\tau_{Sch} = 86.136$ s after fixing $\beta = 0.5$.

From top to bottom, Fig. 2 shows the lensing observables of the hairy EsGB black holes P_{tot}, ΔP, $\Delta F/F_{src}$, and $\Delta\tau$ with respect to the normalized indicator ξ in the left y axis and their deviations from those of the Schwarzschild black hole δP_{tot}, $\delta\Delta P$, $\delta\Delta r$, and $\delta\Delta\tau$ in the right y axis, where we consider five coupling functions $f(\phi) = \{\phi^2, \phi^3, \phi^4, \phi^{-1}, \log(\phi)\}$. P_{tot} for $f(\phi) = \{\phi^2, \phi^3, \phi^4\}$ increase with ξ, while P_{tot} for $f(\phi) = \{\phi^{-1}, \log(\phi)\}$ decrease with it. All of P_{tot} for five coupling functions can reach the level of about 1.1 mas, which is resolvable with current technology, whereas their deviation δP_{tot} from the one of the Schwarzschild black hole is no more than 150 nanoarcsecond (nas), which is far beyond the present ability of astronomical observation. The difference of P_{tot} among the hairy EsGB black holes is even smaller than 20 nas when $\xi \gtrsim 0.1$; nevertheless, P_{tot} for ϕ^{-1} and $\log(\phi)$ can, respectively, differ from the rest of them by about -70 and -150 nas when $\xi \lesssim 0.1$. ΔP for various $f(\phi)$ are all at the level of 270 μas, potentially measurable with existing capacity, but their deviation $\delta\Delta P$ from the one of the Schwarzschild black hole is less than 40 nas, out of the reach of the observations. ΔP and $\delta\Delta P$ for $f(\phi) = \{\phi^{-1}, \log(\phi)\}$ become distinctly bigger than those for $f(\phi) = \{\phi^2, \phi^3, \phi^4\}$ when $\xi \lesssim 0.1$, but all of them are close to each other within about 5 nas when $\xi \gtrsim 0.1$. The pattern of the normalized flux difference $\Delta F/F_{src}$ and its deviation $\delta\Delta r$ from the one of the Schwarzschild black hole is similar to the one of ΔP and $\delta\Delta P$. Although $\Delta F/F_{src}$ is at the level of 0.994 for all of the coupling functions, their deviation $\delta\Delta r$ is never bigger than 10^{-4} mag and the difference $\delta\Delta r$ among various $f(\phi)$ is less than 2×10^{-5} mag for most allowable ξ. It is possible to detect such a $\Delta F/F_{src}$, but $\delta\Delta r$ is beyond the threshold of current photometry. The pattern of $\Delta\tau$ and $\delta\Delta\tau$ is similar to the one of P_{tot} and δP_{tot}. $\Delta\tau$ is about 86.1 s for all $f(\phi)$, their absolute deviation $\delta\Delta\tau$ from the one of the Schwarzschild black hole is less than 12 ms and the difference $\delta\Delta\tau$ among various $f(\phi)$ is less than 2 ms for $\xi \gtrsim 0.1$. Both of the time signals are shorter than the typical time span of an astronomical session, making them inaccessible.

In a summary, after obtaining the observables for Sgr A* in the weak deflection gravitational lensing by the hairy EsGB black holes with various coupling functions, we find that (i) P_{tot}, ΔP, and $\Delta F/F_{src}$ are able to measure but $\Delta\tau$ is not; (ii) the deviations of these observables from those of the Schwarzschild black hole are too small to be detected for now; and (iii) the differences of the observables among various EsGB black holes are even smaller. Therefore, we can conclude that (i) the hairy EsGB black holes cannot be distinguished from the Schwarzschild black hole by the weak deflection gravitational lensing currently, and (ii) it is impossible to tell difference among the hairy EsGB black holes with various coupling functions by the observables of the weak deflection gravitational lensing in the foreseeable future.

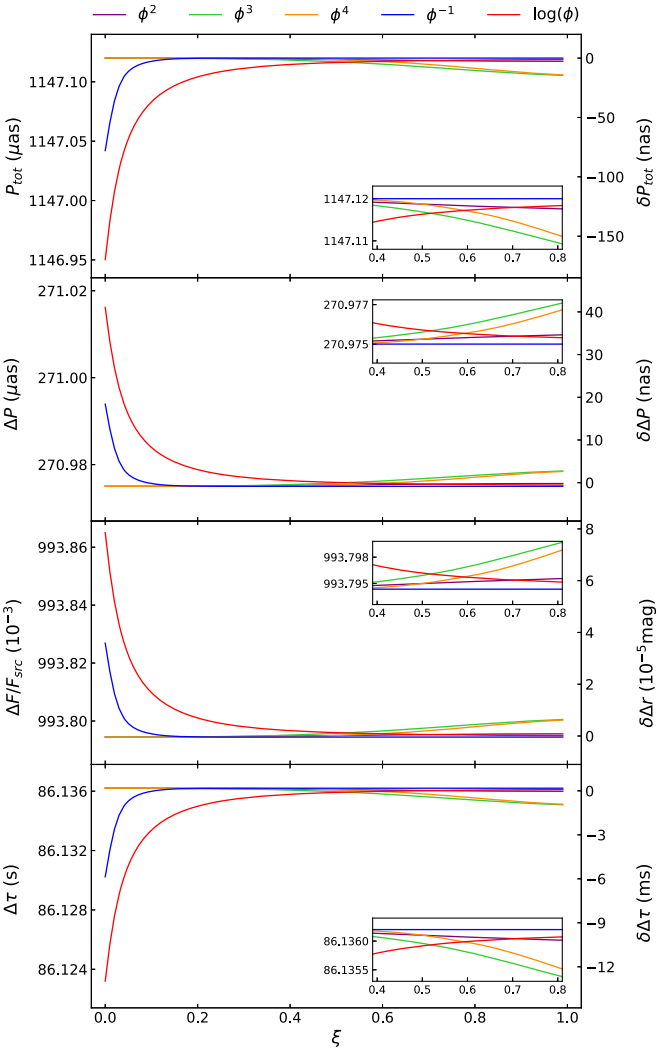

FIG. 2. By taking Sgr A* as the lens, it shows the observables of the weak deflection gravitational lensing by the hairy EsGB black holes with different coupling functions $f(\phi) = \{\phi^2, \phi^3, \phi^4, \phi^{-1}, \log(\phi)\}$ and their deviations from those of the Schwarzschild black hole, where $\beta = 0.5$. For the Schwarzschild black hole, $P_{tot,Sch} = 1.147$ mas, $\Delta P_{Sch} = 0.271$ mas, $\Delta F_{Sch}/F_{src} = 0.994$ and $\Delta\tau_{Sch} = 86.136$ s.

IV. STRONG DEFLECTION GRAVITATIONAL LENSING

When the closest approach distance r_0 of a light ray decreases to the level just a few times bigger than the gravitational radius of a hairy EsGB black hole $\sim 2M$, the photon will wind several times around the lens before arrival at the observer. In such a strong deflection gravitational lensing, the resulting deflection angle $\hat{\alpha}$ will exceed 2π and finally diverge at $r_0 = r_{\rm m}$, where $r_{\rm m}$ is the radius of the photon sphere and is defined as the biggest root to the following equation [58,79]

$$r_{\rm m} \equiv \frac{2A(r_{\rm m})}{A'(r_{\rm m})}, \tag{58}$$

with $'$ being the derivative against r. The impact parameter $b_{\rm m}$ at the photon sphere can be found by Eq. (14) as

$$b_{\rm m} = \frac{r_{\rm m}}{\sqrt{A(r_{\rm m})}}. \tag{59}$$

Using the CFA (4), we can easily obtain $r_{\rm m}$ and $b_{\rm m}$ of the hairy EsGB black holes. In order to evaluate their accuracy, we take the quadratic EsGB gravity as an example and calculate their relative errors between the CFA and numerical approaches. Figure 3 shows that the relative errors of $r_{\rm m}$ and $b_{\rm m}$ are well within 0.3% for $p \lesssim 0.8$ and their overall errors are no more than 2%, demonstrating that the CFA approach is sufficient and reliable for the study on strong deflection gravitational lensing.

A. Strong deflection limit and observables

The deflection angle (13) can be expressed in the logarithmic form in the strong deflection limit as [59,80]

$$\hat{\alpha}(\theta) = -\bar{a}\log\left(\frac{\vartheta d_{\rm L}}{b_{\rm m}} - 1\right) + \bar{b} + \mathcal{O}[(b - b_{\rm m})\log(b - b_{\rm m})] \tag{60}$$

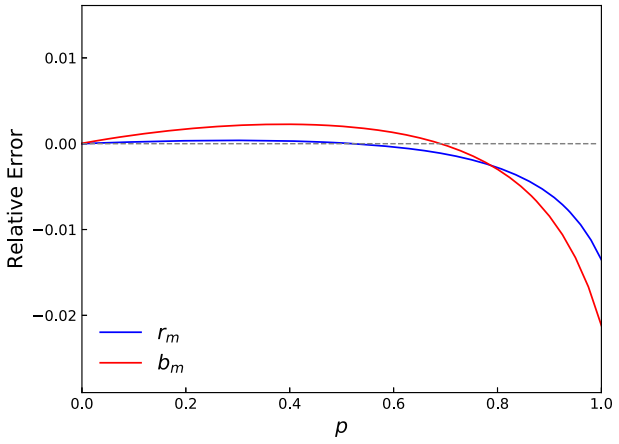

FIG. 3. The relative errors of $r_{\rm m}$ and $b_{\rm m}$ between the CFA and numerical approaches.

where the coefficients are [80]

$$\bar{a} = \sqrt{\frac{2A(r_{\rm m})B(r_{\rm m})}{2A(r_{\rm m}) - r_{\rm m}^2 A''(r_{\rm m})}}, \tag{61}$$

$$\bar{b} = -\pi + \bar{a}\log\left[2 - r_{\rm m}^2\frac{A''(r_{\rm m})}{A(r_{\rm m})}\right] + 2\int_0^1 \left[\sqrt{\frac{A(z)B(z)}{A(r_{\rm m}) - A(z)(1-z)^2}} - \frac{\bar{a}}{z}\right]{\rm d}z, \tag{62}$$

with

$$z = 1 - \frac{r_{\rm m}}{r}. \tag{63}$$

If the source, the lens and the observer are in a nearly collinear alignment and the source and the observer are located in the asymptotically flat spacetime, the lens equation (15) can be simplified as [81]

$$\mathcal{B} = \vartheta - \frac{d_{\rm LS}}{d_{\rm S}}[\hat{\alpha}(\vartheta) - 2n\pi], \tag{64}$$

where n is the looping number of the photon winding around the lens.

The resulting observables in the strong deflection gravitational lensing contain the apparent radius of the photon sphere (the angular size of the shadow) ϑ_∞, the angular separation s, and the brightness difference Δm between the first relativistic image and other packed images, which are [59]

$$\vartheta_\infty = \frac{b_{\rm m}}{d_{\rm L}}, \tag{65}$$

$$s = \vartheta_\infty \exp\left(\frac{\bar{b} - 2\pi}{\bar{a}}\right), \tag{66}$$

$$\Delta m = 2.5\log_{10}\left[\exp\left(\frac{2\pi}{\bar{a}}\right)\right], \tag{67}$$

and the time delay $\Delta T_{2,1}$ between the first two relativistic images, which is [82]

$$\Delta T_{2,1} = 2\pi b_{\rm m} + 2\sqrt{2}\bar{a}b_{\rm m}\exp\left(\frac{\bar{b}}{2\bar{a}}\right) \times \left[\exp\left(-\frac{\pi}{\bar{a}}\right) - \exp\left(-\frac{2\pi}{2\bar{a}}\right)\right]. \tag{68}$$

In order to demonstrate their deviations from those of the Schwarzschild black hole, we define following indicators as

$$\delta\vartheta_\infty = \vartheta_\infty - \vartheta_{\infty,{\rm Sch}}, \tag{69}$$

$$\delta s = s - s_{\rm Sch}, \tag{70}$$

$$\delta\Delta m = \Delta m - \Delta m_{\rm Sch}, \tag{71}$$

$$\delta\Delta T_{2,1} = \Delta T_{2,1} - \Delta T_{2,1,\rm Sch}. \tag{72}$$

The observable with subscripts Sch mean their values for the Schwarzschild black hole which can explicitly be found in Refs. [59,82].

It is worth mentioning that the EHT observation disfavors a nonrotating black hole at the center of M87 and the inferred size of the shadow of M87* is indeed consistent with the prediction based on a Kerr black hole [47]. Nevertheless, it is well known [83–85] that the spin of a black hole has a very weak influence on the size of the shadow. As shown in Ref. [53], the constraints on the parameters in the modified theories of gravity deduced from the observed shadow are only mildly changed when the nonrotating metrics are used. Therefore, although the spins of the hairy black holes in EsGB gravity are neglected in the present work, we can reasonably expect that our following results about the shadows of Sgr A* and M87* are valid at least for the leading order and the EHT observation can also be adopted to test these nonrotating hairy black holes in a sufficiently good manner. Meanwhile, some detailed investigation including the spins will be our next moves.

B. Example of Sgr A*

Taking Sgr A* as the lens, the observables ϑ_∞, s, Δm, and $\Delta T_{2,1}$ of the hairy black holes with different coupling functions $f(\phi) = \{\phi^2, \phi^3, \phi^4, \phi^{-1}, \log(\phi)\}$ in EsGB gravity (the left y axis) and their deviations from those of the Schwarzschild black hole (right y axis) are shown in Fig. 4 from top to bottom. The angular radii of the shadows ϑ_∞ range from 26 to 29 μas for all of these black holes, which could be resolved by EHT in the future. All of these shadows are bigger than that of the Schwarzschild black hole, confirming the results of Ref. [26]. When $\xi \lesssim 0.2$, the black holes with $f(\phi) = \{\phi^{-1}, \log(\phi)\}$ have bigger shadows than others; when $\xi \gtrsim 0.8$, those with $f(\phi) = \{\phi^2, \phi^3, \phi^4\}$ cast larger shadows. Nevertheless, none of their deviations from the one of the Schwarzschild black hole $\delta\vartheta_\infty$ can become more than 2.5 μas, which is currently not resolvable by EHT. It means that although it is possible to detect the shadows of various hairy black holes in EsGB gravity, they are indistinguishable from the one of the Schwarzschild black hole and from each other with the present technology. The angular separations s between the first relativistic image and other packed images for all of these black holes change from 33 to 60 nas, in which the black holes with $f(\phi) = \{\phi^{-1}, \log(\phi)\}$ can have bigger s than others by a factor of 1.5 and 2 as $\xi \approx 0$. Their deviations δs from the one of the Schwarzschild black hole are no more than 30 nas. Both s and δs are far beyond the capacity of present observational resolutions. The brightness differences Δm between the first relativistic image and other packed images for all of these black holes vary from 6.2 to 6.8 mag and their deviations $\delta\Delta m$ from the one of Schwarzschild black hole are smaller than 0.1 mag. Δm and $\delta\Delta m$ show opposite trends with respect to ξ in the comparison of s and δs. The time delay between the first two relativistic images $\Delta T_{2,1}$ can reach the level of 12 min, while their deviations from the Schwarzschild black hole's is shorter than 0.3 min. Both of them are much shorter than the duration of a typical observational session and thus are unable to be measured.

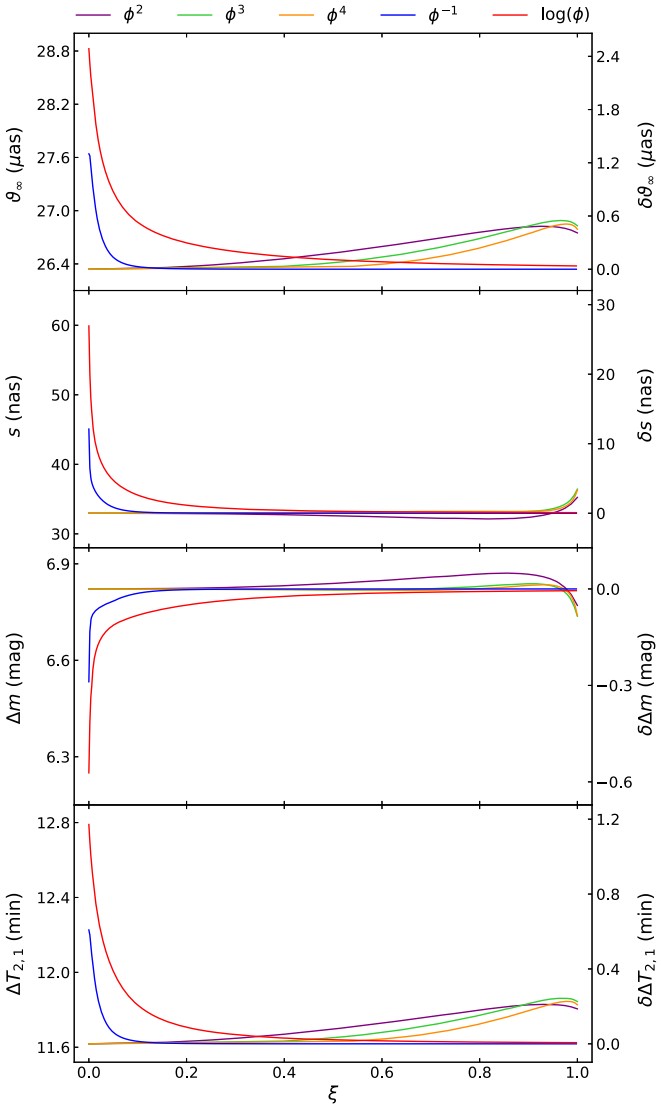

FIG. 4. The observables in the strong deflection gravitational lensing by the hairy EsGB black holes with different coupling functions $f(\phi) = \{\phi^2, \phi^3, \phi^4, \phi^{-1}, \log(\phi)\}$ and their deviations from those of the Schwarzschild black hole are shown by taking Sgr A* as the lens. If Sgr A* is assumed to be a Schwarzschild black hole, then $\vartheta_{\infty,\rm Sch} = 26.4$ μas, $s_{\rm Sch} = 33.0$ nas, $\Delta m_{\rm Sch} = 6.8$ mag, and $\Delta T_{2,1,\rm Sch} = 11.6$ min.

In a summary, after obtaining the observables for Sgr A* in the strong deflection gravitational lensing, we find that (i) the hairy black holes with $f(\phi) = \{\phi^{-1}, \log(\phi)\}$ have more distinctive observables for small ξ and the observables of those with $f(\phi) = \{\phi^2, \phi^3, \phi^4\}$ become more significant as $\xi \approx 1$; (ii) only the apparent sizes of the shadows for these black holes are within the ability of the current technology and none of other observables can be detected in the near future; (iii) the deviations of all observables from those of the Schwarzschild black hole are beyond the reach of the present capacity, making it impossible to distinguish these hairy black holes from the Schwarzschild black hole and from each other.

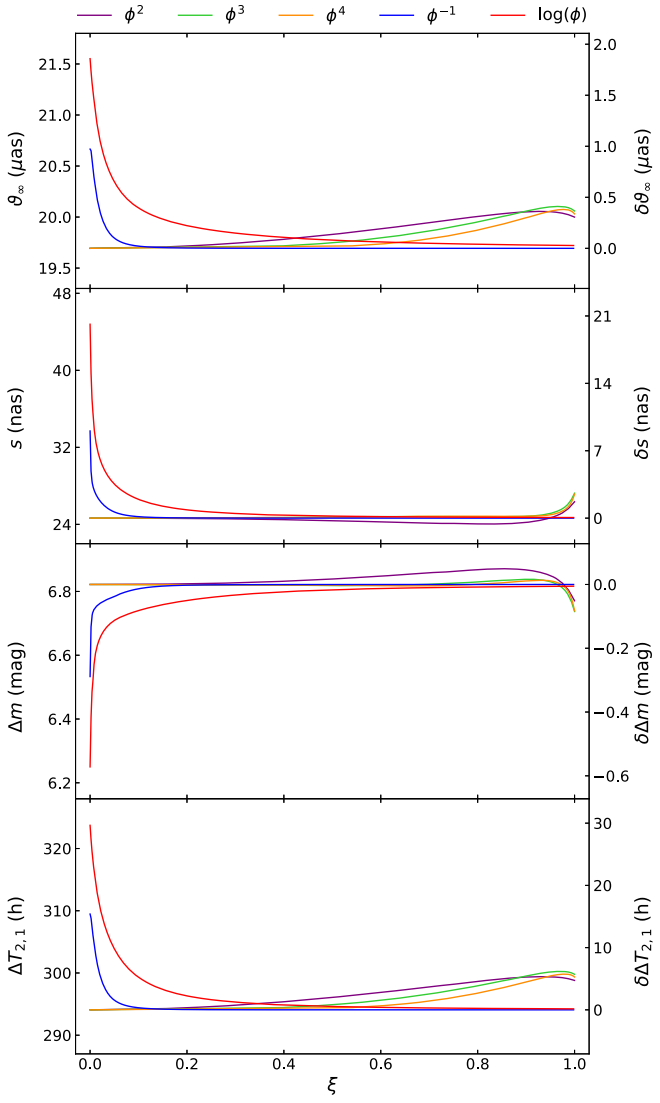

FIG. 5. The observables in the strong deflection gravitational lensing by the hairy EsGB black holes and their deviations from those of the Schwarzschild black hole are shown by taking M87* as the lens. If M87* is assumed to be a Schwarzschild black hole, then $\vartheta_{\infty,\mathrm{Sch}} = 19.7$ μas, $s_{\mathrm{Sch}} = 24.7$ nas, $\Delta m_{\mathrm{Sch}} = 6.8$ mag, and $\Delta T_{2,1,\mathrm{Sch}} = 294$ h.

C. Example of M87*

By taking M87* as the lens with $M = 6.5 \times 10^9$ $M_\odot$ and $d_{\mathrm{L}} = 16.9$ Mpc [52], we find its observables for the hairy EsGB black holes and their deviations from those of the Schwarzschild black hole, shown in Fig. 5. All of these observables and their deviations have the same patterns as those of Sgr A*, in which ϑ_∞, s and $\Delta T_{2,1}$ have different ranges but Δm remain unchanged. The angular radii of the shadows ϑ_∞ for these black holes range from 19.7 to 21.5 μas, which are all consistent with the measured diameter of the M87 shadow 42 ± 3 μas by EHT [47]. But their deviations from the one of the Schwarzschild black hole are within 2 μas, unable to be resolved for now. The angular separations s between the first relativistic image and other packed images for all of these black holes are smaller than 47 nas and their deviations δs from the one of the Schwarzschild black hole are no more than 21 nas, both of which are far beyond the threshold of current astronomical observation. The time delay between the first two relativistic images $\Delta T_{2,1}$ can reach a few hundreds of hours, much longer than those of Sgr A*, while their deviations from the Schwarzschild black hole's change from several to tens of hours. Although both of them are, in principle, able to be measured, the absence of sufficient angular resolution to separate the first two relativistic images makes such a measurement impractical.

In a summary, after assuming M87* as the lens, we find that (i) all the apparent sizes of the shadows cast by these hairy black holes are consistent with the measured one by EHT; and (ii) like the case of Sgr A*, it is currently impossible to distinguish these hairy black holes from the Schwarzschild black hole and from each other by observing the outcome of the strong deflection gravitational lensing of M87*.

V. CONCLUSIONS AND DISCUSSION

In this paper, we investigate the weak and strong deflection gravitational lensing by the black holes with scalar hair in EsGB gravity with coupling functions $f(\phi) = \{\phi^2, \phi^3, \phi^4, \phi^{-1}, \log(\phi)\}$. For the weak deflection gravitational lensing, we obtain the weak deflection angle and resulting observables including the image positions, magnifications and time delay. After taking Sgr A* as the lens, we find that it is possible to measure the angular separation, the angular position difference and the brightness difference between the two lensed images, while it is currently impossible to distinguish the hairy EsGB black holes from the Schwarzschild black hole and from each other according to these observables. For the strong deflection gravitational lensing, we obtain its observables, such as the apparent size of the shadow, the angular image separation, and the brightness difference between the first image and other packed images, and the time delays between the first two relativistic images. By taking Sgr

A* and M87* as the lenses, we find that all of the shadows cast by these black holes are consistent with the measurement by EHT, whereas it is presently infeasible to distinguish them from the Schwarzschild black hole and from each other by these observables.

In the real Universe, astrophysical black holes rotate. Gravitational lensing by spinning hairy EsGB black holes will be an interesting topic for our next move. Based on previous studies in other scenarios [86–102], we could expect their signatures of the gravitational lensing would be more complicated since the spin can make the caustic shifted and distorted. However, to our best knowledge, the analytical form of the metric for these rotating black holes in EsGB gravity is still absent, while the numerical one has been obtained recently [18,103,104]. The CFA method for axisymmetric spacetime [105] might be applied to find a sufficiently good approximation for such a numerical metric. Meanwhile, in order to interpret the observation by EHT, it heavily relies on a bank of the general relativistic magnetohydrodynamics of plasma around the Kerr black hole with a phenomenological prescription for the emission [51]. Nevertheless, these dedicated and highly computational costed simulations are beyond the scope of this work. Although these missing ingredients prevent us from constraining the hairy black holes in EsGB gravity according to the M87*'s shadow in a self-consistent way, our results might still be useful and helpful because they provide observational hints of these black holes which are of the same order of magnitude as those for more realistic cases. Given the fact that gravitational lensing is presently unable to distinguish the hairy EsGB black holes from the Schwarzschild black hole and from each other, the timelike geodesics around these black holes, such as precessing [106–112] and periodic [113–121] orbits, are other important aspects to understand its features.

ACKNOWLEDGMENTS

This work is funded by the National Natural Science Foundation of China (Grant No. 11573015 and No. 11833004) and the Strategic Priority Research Program of Chinese Academy of Sciences (Grant No. XDA15016700).

APPENDIX: CFA COEFFICIENTS

For the hairy black holes in EsGB gravity with coupling functions $f(\phi) = \{\phi^2, \phi^3, \phi^4, \phi^{-1}, \log(\phi)\}$, their CFA coefficients in Eqs. (4), (5), and (6) can be found in the Ref. [26]. We list these coefficients here for self-contained completeness:

(1) $f(\phi) = \phi^2$

$$\epsilon = \frac{-\frac{1}{201}p^2 + \frac{1}{43}p}{-\frac{105}{577}p + 1}, \tag{A1}$$

$$a_1 = \frac{-\frac{23}{143}p^2 + \frac{63}{332}p}{-\frac{83}{401}p^2 + p - \frac{223}{259}}, \tag{A2}$$

$$a_2 = \frac{-\frac{234}{307}p^2 + \frac{152}{397}p + 1}{-\frac{73}{228}p + \frac{73}{221}}, \tag{A3}$$

$$b_1 = \frac{-\frac{85}{438}p^2 + \frac{91}{396}p}{-\frac{24}{131}p^2 + p - \frac{632}{707}}, \tag{A4}$$

$$b_2 = \frac{-\frac{173}{432}p^3 + \frac{47}{225}p^2 - \frac{106}{203}p + 1}{-\frac{25}{283}p + \frac{20}{221}}, \tag{A5}$$

$$\phi_\infty = \frac{-\frac{9}{56}p^2 - \frac{1}{67}p}{p^2 + \frac{38}{61}p + \frac{1}{145}}, \tag{A6}$$

$$f_0 = \frac{-\frac{11}{138}p^3 + \frac{3}{28}p^2 + \frac{1}{113}p}{-\frac{47}{49}p^3 + p^2 + \frac{84}{131}p + \frac{1}{155}}, \tag{A7}$$

$$f_1 = \frac{\frac{63}{151}p^2 + \frac{3}{46}p}{\frac{113}{212}p^2 + p + \frac{2}{111}}, \tag{A8}$$

$$f_2 = \frac{-\frac{23}{55}p^3 - \frac{30}{97}p^2 + p}{\frac{3}{56}p^3 - \frac{31}{79}p^2 + \frac{79}{211}p + \frac{1}{8997}}. \tag{A9}$$

(2) $f(\phi) = \phi^3$

$$\epsilon = \frac{-\frac{1}{186}p^3 + \frac{7}{234}p^2 + \frac{3}{409}p}{p + \frac{34}{271}}, \tag{A10}$$

$$a_1 = \frac{-\frac{79}{638}p^2 + \frac{11}{84}p}{-\frac{124}{405}p^2 + p - \frac{233}{328}}, \tag{A11}$$

$$a_2 = \frac{-\frac{179}{182}p^3 + p^2 + \frac{97}{253}p}{-\frac{41}{212}p^2 + \frac{41}{209}p + \frac{1}{360}}, \tag{A12}$$

$$b_1 = \frac{-\frac{58}{301}p^2 + \frac{33}{145}p}{-\frac{77}{414}p^2 + p - \frac{217}{244}}, \tag{A13}$$

$$b_2 = \frac{p^3 - \frac{119}{205}p^2 - \frac{186}{227}p - \frac{1}{123}}{\frac{19}{181}p^2 - \frac{86}{811}p - \frac{1}{512}}, \tag{A14}$$

$$\phi_\infty = \frac{\frac{1}{59}p^3 - \frac{10}{91}p^2 + \frac{5}{77}p}{\frac{66}{83}p^2 + p + \frac{1}{1087}}, \tag{A15}$$

$$f_0 = \frac{-\frac{1}{142}p^3 + \frac{7}{43}p^2 + \frac{2}{111}p}{p^2 + \frac{29}{75}p + \frac{1}{312}}, \tag{A16}$$

$$f_1 = \frac{\frac{46}{91}p^2 + \frac{11}{138}p}{\frac{101}{146}p^2 + p + \frac{2}{119}}, \tag{A17}$$

$$f_2 = \frac{-\frac{63}{80}p^3 + \frac{8}{117}p^2 + p + \frac{4}{143}}{\frac{8}{93}p^3 - \frac{51}{95}p^2 + \frac{59}{127}p + \frac{2}{69}}. \tag{A18}$$

(3) $f(\phi) = \phi^4$

$$\epsilon = \frac{\frac{8}{247}p^2 + \frac{2}{331}p}{\frac{111}{305}p^2 + p + \frac{28}{311}}, \tag{A19}$$

$$a_1 = \frac{-\frac{115}{804}p^3 + \frac{13}{84}p^2 + \frac{1}{153}p}{-\frac{85}{317}p^3 + p^2 - \frac{168}{233}p - \frac{13}{239}}, \tag{A20}$$

$$a_2 = \frac{-\frac{207}{218}p^3 + p^2 + \frac{85}{278}p - \frac{1}{672}}{-\frac{57}{379}p^2 + \frac{43}{283}p + \frac{1}{359}}, \tag{A21}$$

$$b_1 = \frac{-\frac{26}{135}p^2 + \frac{53}{233}p}{-\frac{73}{393}p^2 + p - \frac{282}{317}}, \tag{A22}$$

$$b_2 = \frac{p^3 - \frac{288}{397}p^2 - \frac{197}{308}p - \frac{1}{142}}{\frac{39}{467}p^2 - \frac{32}{381}p - \frac{1}{516}}, \tag{A23}$$

$$\phi_\infty = \frac{\frac{1}{33}p^2 + \frac{4}{27}p}{p^2 + \frac{193}{225}p + \frac{1}{1136}}, \tag{A24}$$

$$f_0 = \frac{-\frac{1}{140}p^3 + \frac{21}{136}p^2 + \frac{p}{61}}{p^2 + \frac{29}{88}p + \frac{1}{380}}, \tag{A25}$$

$$f_1 = \frac{\frac{99}{188}p^2 + \frac{11}{137}p}{\frac{115}{182}p^2 + p + \frac{1}{62}}, \tag{A26}$$

$$f_2 = \frac{-\frac{32}{103}p^4 + p^3 - \frac{39}{59}p^2 - \frac{92}{307}p}{\frac{17}{97}p^2 - \frac{4}{19}p - \frac{1}{1003}}. \tag{A27}$$

(4) $f(\phi) = \phi^{-1}$

$$\epsilon = \frac{-\frac{2}{317}p^3 + \frac{25}{341}p^2 + \frac{8}{147}p}{p + \frac{167}{308}}, \tag{A28}$$

$$a_1 = \frac{\frac{13}{121}p^3 - \frac{4}{49}p^2 - \frac{16}{281}p}{\frac{11}{355}p^2 - \frac{245}{263}p + 1}, \tag{A29}$$

$$a_2 = \frac{-\frac{583}{875}p^3 + p^2 - \frac{31}{292}p - \frac{13}{367}}{-\frac{57}{340}p^2 + \frac{49}{306}p + \frac{2}{161}}, \tag{A30}$$

$$b_1 = \frac{-\frac{75}{406}p^2 + \frac{103}{477}p}{-\frac{12}{59}p^2 + p - \frac{165}{191}}, \tag{A31}$$

$$b_2 = \frac{-\frac{300}{307}p^2 + \frac{585}{1756}p + 1}{\frac{25}{182}p^2 - \frac{133}{257}p + \frac{259}{671}}, \tag{A32}$$

$$\phi_\infty = \frac{-\frac{25}{84}p^3 + p^2 + \frac{31}{113}p + \frac{1}{181}}{-\frac{11}{69}p^3 + \frac{43}{84}p^2 + \frac{7}{83}p + \frac{1}{1297}}, \tag{A33}$$

$$f_0 = \frac{-\frac{1}{71}p^3 - \frac{28}{71}p^2 - \frac{5}{141}p}{p^2 + \frac{27}{58}p + \frac{1}{198}}, \tag{A34}$$

$$f_1 = \frac{-\frac{10}{143}p^3 - \frac{27}{190}p^2 - \frac{1}{194}p}{p^2 + \frac{2}{15}p + \frac{1}{1496}}, \tag{A35}$$

$$f_2 = \frac{\frac{3}{16}p^3 - \frac{7}{81}p^2 - \frac{7}{71}p - \frac{1}{46}}{-\frac{41}{97}p^3 + p^2 - \frac{121}{230}p - \frac{1}{17}}. \tag{A36}$$

(5) $f(\phi) = \log(\phi)$

$$\epsilon = \frac{-\frac{44}{1323}p^2 + \frac{105}{1018}p}{-\frac{349}{657}p + 1}, \tag{A37}$$

$$a_1 = \frac{\frac{11}{761}p^3 - \frac{113}{2844}p^2 + \frac{18}{709}p}{-\frac{605}{1314}p^2 + p - \frac{425}{787}}, \tag{A38}$$

$$a_2 = \frac{-\frac{586}{813}p^3 + \frac{367}{666}p^2 + p - \frac{384}{611}}{-\frac{255}{1189}p + \frac{237}{1072}}, \tag{A39}$$

$$b_1 = \frac{-\frac{57}{308}p^2 + \frac{85}{387}p}{-\frac{29}{152}p^2 + p - \frac{222}{251}}, \tag{A40}$$

$$b_2 = \frac{-\frac{66}{197}p^2 + p - \frac{262}{383}}{-\frac{73}{318}p^2 + \frac{149}{295}p - \frac{69}{250}}, \tag{A41}$$

$$\phi_\infty = \frac{-\frac{277}{405}p^3 + \frac{159}{218}p^2 + p + \frac{10}{253}}{-\frac{37}{458}p^3 + \frac{167}{246}p^2 + \frac{73}{608}p + \frac{1}{1310}}, \tag{A42}$$

$$f_0 = \frac{\frac{140}{449}p^3 + \frac{58}{271}p^2 + \frac{1}{232}p}{p^2 + \frac{25}{214}p + \frac{1}{3196}}, \tag{A43}$$

$$f_1 = \frac{-\frac{83}{188}p^3 + \frac{160}{239}p^2 + \frac{28}{285}p}{-\frac{269}{372}p^2 + p + \frac{3}{148}}, \tag{A44}$$

$$f_2 = \frac{\frac{81}{203}p^3 + \frac{37}{378}p^2 - \frac{350}{571}p - \frac{29}{802}}{-\frac{139}{605}p^3 + p^2 - \frac{173}{233}p - \frac{31}{384}}. \tag{A45}$$

[1] D. J. Gross and J. H. Sloan, Nucl. Phys. **B291**, 41 (1987).
[2] M. Gasperini and G. Veneziano, Astropart. Phys. **1**, 317 (1993).
[3] T. Kobayashi, M. Yamaguchi, and J. Yokoyama, Prog. Theor. Phys. **126**, 511 (2011).
[4] E. Berti *et al.*, Classical Quantum Gravity **32**, 243001 (2015).
[5] B. Zwiebach, Phys. Lett. **156B**, 315 (1985).
[6] P. Kanti, N. E. Mavromatos, J. Rizos, K. Tamvakis, and E. Winstanley, Phys. Rev. D **54**, 5049 (1996).
[7] B. Kleihaus, J. Kunz, S. Mojica, and E. Radu, Phys. Rev. D **93**, 044047 (2016).
[8] T. P. Sotiriou and S.-Y. Zhou, Phys. Rev. Lett. **112**, 251102 (2014).
[9] T. P. Sotiriou and S.-Y. Zhou, Phys. Rev. D **90**, 124063 (2014).
[10] G. Antoniou, A. Bakopoulos, and P. Kanti, Phys. Rev. Lett. **120**, 131102 (2018).
[11] D. D. Doneva and S. S. Yazadjiev, Phys. Rev. Lett. **120**, 131103 (2018).
[12] H. O. Silva, J. Sakstein, L. Gualtieri, T. P. Sotiriou, and E. Berti, Phys. Rev. Lett. **120**, 131104 (2018).
[13] H. O. Silva, C. F. B. Macedo, T. P. Sotiriou, L. Gualtieri, J. Sakstein, and E. Berti, Phys. Rev. D **99**, 064011 (2019).
[14] M. Minamitsuji and T. Ikeda, Phys. Rev. D **99**, 044017 (2019).
[15] M. Minamitsuji and T. Ikeda, Phys. Rev. D **99**, 104069 (2019).
[16] Y.-X. Gao, Y. Huang, and D.-J. Liu, Phys. Rev. D **99**, 044020 (2019).
[17] C. A. R. Herdeiro, E. Radu, N. Sanchis-Gual, and J. A. Font, Phys. Rev. Lett. **121**, 101102 (2018).
[18] P. V. P. Cunha, C. A. R. Herdeiro, and E. Radu, Phys. Rev. Lett. **123**, 011101 (2019).
[19] J. L. Blázquez-Salcedo, D. D. Doneva, J. Kunz, and S. S. Yazadjiev, Phys. Rev. D **98**, 084011 (2018).
[20] J. L. Blázquez-Salcedo, D. D. Doneva, S. Kahlen, J. Kunz, P. Nedkova, and S. S. Yazadjiev, Phys. Rev. D **101**, 104006 (2020).
[21] J. L. Blázquez-Salcedo, D. D. Doneva, S. Kahlen, J. Kunz, P. Nedkova, and S. S. Yazadjiev, Phys. Rev. D **102**, 024086 (2020).
[22] O. J. Tattersall, P. G. Ferreira, and M. Lagos, Phys. Rev. D **97**, 084005 (2018).
[23] B. P. Abbott, R. Abbott, T. D. Abbott, F. Acernese, K. Ackley, C. Adams, T. Adams, P. Addesso, R. X. Adhikari, V. B. Adya *et al.*, Phys. Rev. Lett. **119**, 161101 (2017).
[24] B. P. Abbott, R. Abbott, T. D. Abbott, F. Acernese, K. Ackley, C. Adams, T. Adams, P. Addesso, R. X. Adhikari, V. B. Adya *et al.*, Astrophys. J. Lett. **848**, L12 (2017).
[25] P. V. P. Cunha, C. A. R. Herdeiro, B. Kleihaus, J. Kunz, and E. Radu, Phys. Lett. B **768**, 373 (2017).
[26] R. A. Konoplya, T. Pappas, and A. Zhidenko, Phys. Rev. D **101**, 044054 (2020).
[27] L. Rezzolla and A. Zhidenko, Phys. Rev. D **90**, 084009 (2014).
[28] V. Perlick, Living Rev. Relativity **7**, 9 (2004).
[29] P. Schneider, J. Ehlers, and E. E. Falco, *Gravitational Lenses* (Springer-Verlag, Berlin, 1992).
[30] A. O. Petters, H. Levine, and J. Wambsganss, *Singularity Theory and Gravitational Lensing* (Birkhäuser, Boston, 2001).
[31] P. Schneider, C. S. Kochanek, and J. Wambsganss, in *Saas-Fee Advanced Course 33: Gravitational Lensing: Strong, Weak and Micro*, edited by G. Meylan, P. Jetzer, and P. North (Springer-Verlag, Berlin, 2006).
[32] K. C. Sahu, J. Anderson, S. Casertano, H. E. Bond, P. Bergeron, E. P. Nelan, L. Pueyo, T. M. Brown, A. Bellini, Z. G. Levay, J. Sokol, M. Dominik, A. Calamida, N. Kains, and M. Livio, Science **356**, 1046 (2017).
[33] C. R. Keeton and A. O. Petters, Phys. Rev. D **72**, 104006 (2005).
[34] C. R. Keeton and A. O. Petters, Phys. Rev. D **73**, 044024 (2006).
[35] C. R. Keeton and A. O. Petters, Phys. Rev. D **73**, 104032 (2006).
[36] T. E. Collett, L. J. Oldham, R. J. Smith, M. W. Auger, K. B. Westfall, D. Bacon, R. C. Nichol, K. L. Masters, K. Koyama, and R. van den Bosch, Science **360**, 1342 (2018).
[37] G. Li and X.-M. Deng, Ann. Phys. (Amsterdam) **382**, 136 (2017).
[38] Y. Xie, Phys. Rev. D **98**, 021501(R) (2018).
[39] W.-G. Cao and Y. Xie, Eur. Phys. J. C **78**, 191 (2018).
[40] J. L. Synge, Mon. Not. R. Astron. Soc. **131**, 463 (1966).
[41] C. Darwin, Proc. R. Soc. A **249**, 180 (1959).
[42] V. Bozza, Gen. Relativ. Gravit. **42**, 2269 (2010).
[43] P. V. P. Cunha and C. A. R. Herdeiro, Gen. Relativ. Gravit. **50**, 42 (2018).
[44] S. E. Gralla, D. E. Holz, and R. M. Wald, Phys. Rev. D **100**, 024018 (2019).
[45] M. D. Johnson, A. Lupsasca, A. Strominger, G. N. Wong, S. Hadar, D. Kapec, R. Narayan, A. Chael, C. F. Gammie, P. Galison, D. C. M. Palumbo, S. S. Doeleman, L. Blackburn, M. Wielgus, D. W. Pesce, J. R. Farah, and J. M. Moran, Sci. Adv. **6**, eaaz1310 (2020).
[46] S. E. Gralla and A. Lupsasca, Phys. Rev. D **102**, 124003 (2020).
[47] Event Horizon Telescope Collaboration, Astrophys. J. Lett. **875**, L1 (2019).
[48] Event Horizon Telescope Collaboration, Astrophys. J. Lett. **875**, L2 (2019).
[49] Event Horizon Telescope Collaboration, Astrophys. J. Lett. **875**, L3 (2019).
[50] Event Horizon Telescope Collaboration, Astrophys. J. Lett. **875**, L4 (2019).
[51] Event Horizon Telescope Collaboration, Astrophys. J. Lett. **875**, L5 (2019).
[52] Event Horizon Telescope Collaboration, Astrophys. J. Lett. **875**, L6 (2019).
[53] Event Horizon Telescope Collaboration, Phys. Rev. Lett. **125**, 141104 (2020).
[54] S. E. Gralla, Phys. Rev. D **103**, 024023 (2021).
[55] S. H. Völkel, E. Barausse, N. Franchini, and A. E. Broderick, arXiv:2011.06812.
[56] K. S. Virbhadra, D. Narasimha, and S. M. Chitre, Astron. Astrophys. **337**, 1 (1998), https://ui.adsabs.harvard.edu/abs/1998A%26A...337....1V/abstract.
[57] A. O. Petters, Mon. Not. R. Astron. Soc. **338**, 457 (2003).

[58] K. S. Virbhadra and G. F. R. Ellis, Phys. Rev. D **62**, 084003 (2000).
[59] V. Bozza, Phys. Rev. D **66**, 103001 (2002).
[60] V. Bozza, Phys. Rev. D **67**, 103006 (2003).
[61] S. E. Vázquez and E. P. Esteban, Nuovo Cimento B **119**, 489 (2004).
[62] A. Y. Bin-Nun, Phys. Rev. D **81**, 123011 (2010).
[63] G. N. Gyulchev and I. Z. Stefanov, Phys. Rev. D **87**, 063005 (2013).
[64] S.-S. Zhao and Y. Xie, J. Cosmol. Astropart. Phys. 07 (2016) 007.
[65] X. Lu, F.-W. Yang, and Y. Xie, Eur. Phys. J. C **76**, 357 (2016).
[66] S. Chakraborty and S. SenGupta, J. Cosmol. Astropart. Phys. 07 (2017) 045.
[67] S. E. Gralla, A. Lupsasca, and D. P. Marrone, Phys. Rev. D **102**, 124004 (2020).
[68] Z. Horváth, L. Á. Gergely, Z. Keresztes, T. Harko, and F. S. N. Lobo, Phys. Rev. D **84**, 083006 (2011).
[69] E. F. Eiroa and C. M. Sendra, Phys. Rev. D **86**, 083009 (2012).
[70] R. N. Izmailov, R. K. Karimov, E. R. Zhdanov, and K. K. Nandi, Mon. Not. R. Astron. Soc. **483**, 3754 (2019).
[71] C.-Y. Wang, Y.-F. Shen, and Y. Xie, J. Cosmol. Astropart. Phys. 04 (2019) 022.
[72] F.-Y. Liu, Y.-F. Mai, W.-Y. Wu, and Y. Xie, Phys. Lett. B **795**, 475 (2019).
[73] X. Lu and Y. Xie, Eur. Phys. J. C **79**, 1016 (2019).
[74] X. Lu and Y. Xie, Eur. Phys. J. C **80**, 625 (2020).
[75] G. Antoniou, A. Bakopoulos, and P. Kanti, Phys. Rev. D **97**, 084037 (2018).
[76] S. Weinberg, *Gravitation and Cosmology: Principles and Applications of the General Theory of Relativity* (Wiley, New York, 1972).
[77] S. Refsdal, Mon. Not. R. Astron. Soc. **128**, 295 (1964).
[78] S. Gillessen, P. M. Plewa, F. Eisenhauer, R. Sari *et al.*, Astrophys. J. **837**, 30 (2017).
[79] C.-M. Claudel, K. S. Virbhadra, and G. F. R. Ellis, J. Math. Phys. (N.Y.) **42**, 818 (2001).
[80] N. Tsukamoto, Phys. Rev. D **95**, 064035 (2017).
[81] V. Bozza, S. Capozziello, G. Iovane, and G. Scarpetta, Gen. Relativ. Gravit. **33**, 1535 (2001).
[82] V. Bozza and L. Mancini, Gen. Relativ. Gravit. **36**, 435 (2004).
[83] T. Johannsen and D. Psaltis, Astrophys. J. **718**, 446 (2010).
[84] T. Johannsen, Astrophys. J. **777**, 170 (2013).
[85] L. Medeiros, D. Psaltis, and F. Özel, Astrophys. J. **896**, 7 (2020).
[86] J. Ibanez, Astron. Astrophys. **124**, 175 (1983), https://ui.adsabs.harvard.edu/abs/1983A%26A...124..175I/abstract.
[87] I. Bray, Phys. Rev. D **34**, 367 (1986).
[88] S. A. Klioner, Sov. Astron. **35**, 523 (1991), https://ui.adsabs.harvard.edu/abs/1991SvA....35..523K/abstract.
[89] J. F. Glicenstein, Astron. Astrophys. **343**, 1025 (1999), https://ui.adsabs.harvard.edu/abs/1999A%26A...343.1025G/abstract.
[90] M. Sereno and F. De Luca, Phys. Rev. D **74**, 123009 (2006).
[91] M. C. Werner and A. O. Petters, Phys. Rev. D **76**, 064024 (2007).
[92] M. Sereno and F. De Luca, Phys. Rev. D **78**, 023008 (2008).
[93] A. B. Aazami, C. R. Keeton, and A. O. Petters, J. Math. Phys. (N.Y.) **52**, 092502 (2011).
[94] A. B. Aazami, C. R. Keeton, and A. O. Petters, J. Math. Phys. (N.Y.) **52**, 102501 (2011).
[95] G. He and W. Lin, Int. J. Mod. Phys. D **23**, 1450031 (2014).
[96] G. He, C. Jiang, and W. Lin, Int. J. Mod. Phys. D **23**, 1450079 (2014).
[97] X.-M. Deng, Int. J. Mod. Phys. D **24**, 1550056 (2015).
[98] G.-S. He and W.-B. Lin, Res. Astron. Astrophys. **15**, 646 (2015).
[99] X.-M. Deng, Int. J. Mod. Phys. D **25**, 1650082 (2016).
[100] G. He and W. Lin, Phys. Rev. D **93**, 023005 (2016).
[101] G. He and W. Lin, Phys. Rev. D **94**, 063011 (2016).
[102] G. He and W. Lin, Classical Quantum Gravity **34**, 105006 (2017).
[103] C. A. R. Herdeiro, E. Radu, H. O. Silva, T. P. Sotiriou, and N. Yunes, Phys. Rev. Lett. **126**, 011103 (2021).
[104] E. Berti, L. G. Collodel, B. Kleihaus, and J. Kunz, Phys. Rev. Lett. **126**, 011104 (2021).
[105] R. Konoplya, L. Rezzolla, and A. Zhidenko, Phys. Rev. D **93**, 064015 (2016).
[106] M. De Laurentis, R. De Rosa, F. Garufi, and L. Milano, Mon. Not. R. Astron. Soc. **424**, 2371 (2012).
[107] X.-M. Deng, Europhys. Lett. **120**, 60004 (2017).
[108] X.-M. Deng, Eur. Phys. J. Plus **132**, 85 (2017).
[109] I. De Martino, R. Lazkoz, and M. De Laurentis, Phys. Rev. D **97**, 104067 (2018).
[110] M. De Laurentis, I. De Martino, and R. Lazkoz, Phys. Rev. D **97**, 104068 (2018).
[111] M. De Laurentis, I. De Martino, and R. Lazkoz, Eur. Phys. J. C **78**, 916 (2018).
[112] T.-Y. Zhou and Y. Xie, Eur. Phys. J. C **80**, 1070 (2020).
[113] J. Levin and G. Perez-Giz, Phys. Rev. D **77**, 103005 (2008).
[114] J. Levin and R. Grossman, Phys. Rev. D **79**, 043016 (2009).
[115] J. Levin and G. Perez-Giz, Phys. Rev. D **79**, 124013 (2009).
[116] J. Levin, Classical Quantum Gravity **26**, 235010 (2009).
[117] V. Misra and J. Levin, Phys. Rev. D **82**, 083001 (2010).
[118] B. Gao and X.-M. Deng, Ann. Phys. (Amsterdam) **418**, 168194 (2020).
[119] X.-M. Deng, Eur. Phys. J. C **80**, 489 (2020).
[120] X.-M. Deng, Phys. Dark Universe **30**, 100629 (2020).
[121] H.-Y. Lin and X.-M. Deng, Phys. Dark Universe **31**, 100745 (2021).